Resilient Microgrid Scheduling with Secure Frequency and Voltage Transient Response

Agnes M. Nakiganda, *Graduate Student Member, IEEE*, Petros Aristidou, *Senior Member, IEEE*

Abstract—The resilient operation of microgrids (MGs) relies strongly on their ability to operate in islanded mode, autonomously from the bulk grid, whilst adhering to secure operation requirements. Catastrophic events in the transmission grid can lead to abrupt MG islanding accommodated by large frequency and voltage excursions due to power imbalances within the MG. It is vital that MG scheduling algorithms incorporate both static and transient security metrics to ensure a secure transition during islanding, immunised against the transient phenomena. In this paper, we incorporate both frequency- and voltage-related security constraints in a MG operational planning problem to ensure robust operation against abrupt islanding events. We employ an iterative dynamic optimization approach, based on the sensitivities of active and reactive power injections to the system security metrics, to incorporate the transient and static security constraints in the planning problem. Due to their non-linear and intractable nature, the transient security constraints are reformulated as linear sequential resilience cuts resulting in a computationally efficient problem. The performance of the algorithm is shown on a 30-bus, 20 kV, distribution network, subject to a 24-hour variation in load and renewable generation.

Index Terms—Frequency security, low-inertia systems, operational planning, unscheduled islanding, voltage security, microgrids

Nomenclature

Acronyms

CIGs	Converter-Interfaced GeneratorS
CoI	Center-of-Inertia
DAD	Differential-Algebraic-Discrete
DERs	Distributed Energy ResourceS
FRT	Fault Ride-Through
HILF	High Impact Low Frequency
IR	Inertial Response
L/HVRT	Low/High Voltage Ride-Through
MG	Microgrid
PCC	Point-of-Common-Coupling
PFR	Primary Frequency Response
RfG	Requirements for GeneratorS
RoCoF	Rate-of-change of Frequency
SGs	Synchronous Generators
VSM	Virtual Synchronous Machine

Functions

A. Nakiganda is with the Center for Electric Power and Energy at the Technical University of Denmark (DTU), Lyngby, Denmark (amanak@dtu.dk).

P. Aristidou is with the Department of Electrical Engineering, Computer Engineering, and Informatics, Cyprus University of Technology, Cyprus (petros.aristidou@cut.ac.cy).

$\Theta^{\mathbf{gm}}$	Total operational costs in grid-connected mode [$].
$\Theta_t^{\mathbf{im}}$	Total penalty costs of disconnecting loads from MG at hour t in islanded mode [$].

Indices

c	Index of CIG.
s	Index of SG.
g	Index of generators, $g \in \{c, s\}$.
i	Index of nodes, $\eta(l^+)/\eta(l^-)$ being a node upstream/downstream of node i.
t	Index of hours.
k	Index of iterations.
l	Index of lines, where (l^+) denotes the sending end and (l^-) is the receiving end.

Parameters

$C^{\mathrm{imp}^{P/Q}}/C^{\mathrm{exp}^{P/Q}}$	Buying/selling price of electricity from/to the main grid [$/kWh]/[$/kVarh].
C_d^{v}	Penalty cost of shifting load d [$/kWh].
C_d	Penalty cost of curtailing load d during islanded operation [$/kWh].
$C_g^{P/Q}$	Power generation and operational cost of generator g [$/kWh].
$E_s^{\mathrm{FR,max}}$	Maximum energy reserve limit for transient frequency support for generator g [kWh].
E_d	Total energy demand for load d in planning horizon $\mathcal{T}$ [kWh].
r_l	Resistance of the line l, [Ω].
rd/ru_s	Ramp-down/ramp-up limit of generator s [kW/h].
x_l	Reactance of the line l, [Ω].
$y_{l^{+/-}}^{sh}$	Shunt admittance at the sending/receiving ends of the line l, [S].
y_l^s	Series admittance of the line l where $y_l = 1/z_l$, [S].
z_l	Impedance of the line l, where $z_l = (r_l + \mathbf{j}x_l)$ [Ω].

Sets

$\mathcal{C}$	Set nodes with CIGs, where $\mathcal{C}^i$ is the set of generators connected to node i and $\mathcal{C} \subseteq \mathcal{N}$.
$\mathcal{D}$	Set of nodes with loads, where $\mathcal{D}^i$ is the set of loads connected to node i and $\mathcal{D} \subseteq \mathcal{N}$.
$\mathcal{L}$	Set of lines connecting neighbouring nodes. Lines connected downstream to a node are included in set $\mathcal{L}^{\eta(l^+)}$ while those connected upstream to a node are included in set $\mathcal{L}^{\eta(l^-)}$, and $\mathcal{L} \subseteq \mathcal{N} \times \mathcal{N}$.
$\mathcal{N}$	Set of all nodes, where $\mathcal{N}^i$ is the set of nodes after and connected to node i.
$\mathcal{M}$	Set of nodes with generators, where $\mathcal{M}^i$ is the set of all generators connected to node i and $\mathcal{M} := \mathcal{S} \cup \mathcal{C}$.

$\mathcal{S}$ Set of nodes with SGs, where $\mathcal{S}^i$ is the set of generators connected to node i and $\mathcal{S} \subseteq \mathcal{N}$.

$\mathcal{T}$ Set of hours in the planning horizon.

Symbols

$\underline{\bullet}/\overline{\bullet}$ Lower/upper bounds of the quantity $\bullet$.

$|\bullet|$ Cardinality of the set $\bullet$.

Variables

$f_{tl_{+/-}}$ Square of current magnitude at flowing into line l from the sending/receiving end at hour t $[A^2]$.

$p/q_t^{\mathrm{imp/exp}}$ Active/reactive power imported/exported from/to the main grid at hour t [kW/kVAr].

p/q_{dt} Active/reactive load power for load d and hour t [kW/kVAr].

p/q_{dt}^{f} Fixed part of active/reactive load power for load d at hour t [kW/kVAr].

p/q_{dt}^{v} Variable part of active/reactive load power for load d at hour t [kW/kVAr].

p/q_{gt} Active/reactive power generation of generator g at hour t [kW/kVAr].

p_g^{FR} Active power reserve for transient frequency support of generator g [kW].

$P_{tl_{+/-}}$ Active power flow into line l from the sending$(+)$/receiving$(-)$ end at hour t [kW].

$Q_{tl_{+/-}}$ Reactive power flow into line l from the sending$(+)$/receiving$(-)$ end at hour t [kVAr].

s_t^{grid} Apparent power injection from the main grid at hour t, $s^{\mathrm{imp}}/s^{\mathrm{exp}}$ being the apparent power imported/exported from/to the main grid, [kVA].

s_{it} Apparent power injection at node i for hour t, where $s_{it} = p_{it} + \mathbf{j}q_{it}$, [kVA].

$S_{tl_{+/-}}$ Apparent power flow into line l at the sending/receiving end for hour t, where $S_{l+} = P_{l+} + \mathbf{j}Q_{l+}$ ($S_{l-} = P_{l-} + \mathbf{j}Q_{l-}$), [kVA].

v_{it} Square of voltage magnitude at node i at hour t $[V^2]$.

z_{dt} Binary variable indicating the connection status of load d at hour t (i.e., $1/0$: connected/disconnected).

$z_t^{\mathrm{P/Q}}$ Binary variable indicating active/reactive power import or export from the grid (i.e., $1/0$: import/export).

Vectors

$\boldsymbol{\mu}$ Vector of all performance metrics.

$\boldsymbol{u}$ Vector of all control variables.

$\boldsymbol{x}$ Vector of differential state variables.

$\boldsymbol{y}$ Vector of all steady-state operational variables.

I. Introduction

THE prevalence of extreme events affecting the power system has significantly increased in the last decade. High Impact Low Frequency (HILF) events such as extreme weather conditions or significant faults in power networks, can result in disruptions and failures in the transmission and distribution networks. To mitigate the negative effects, it is required to have diversity and flexibility in the power supply. Microgrids (MGs) have been widely considered as a potential solution for enhancing the system survivability and resilience by exploiting the flexibility potential available in the MG Distributed Energy Resources (DERs) [1, 2]. Additionally, MGs hold the capability to operate in coexistence with the bulk grid or as self-sufficient islands able to ensure supply continuance to local demand, namely in grid-connected or islanded modes.

In the event of HILF events, the capability of MGs to successfully move from grid-connected to islanded mode and ensure supply continuity is critical in enhancing the system resilience. The islanding process might fail due to inadequacy in power supply capacity, loss of synchronisation for grid-connected converters, and the action of generator protections resulting in unit disconnections. Notably, the large transient excursions in the MG voltage and frequency during the abrupt transition can affect the MG's operational integrity [3, 4]. If not adequately addressed, the transient phenomena can lead to cascading failures and destabilise the MG.

However, with the increasing integration of Converter-Interfaced Generators (CIGs), it becomes more demanding to ensure system security. While the fast-acting CIGs have numerous advantages, the replacement of Synchronous Generators (SGs) results in a radical transformation of the dynamic response and operational characteristics of the system; affecting both voltage and frequency security during fault conditions [5]. Therefore, it is necessary that DERs provide grid-supporting services, including frequency control, inertia support, reactive power support, and voltage control, to ensure operational stability and security during emergency conditions.

Traditionally, operational planning problems for MGs in grid-connected and islanded modes have focused on the network behaviour in pre- and post-contingency steady states [6–8]. This approach ensures self-sufficiency and steady-state stability but neglects the transient security during system transition. The works in [9, 10] have analysed the frequency and voltage security in steady-state but neglect the transient response. More recently studies have introduced "transient-aware" planning approaches aiming to provide preventive-control solutions and mitigate the effects of large transient excursions during HILF events. In [11–16], analytical formulations of the frequency security metrics have been developed based on a reduced-order single machine equivalent Centre-of-Inertia (CoI) frequency model. In [11, 12], unit commitment and economic dispatch problems are proposed for networks with only conventional generators, incorporating security constraints based on linearised analytical formulations of frequency metrics. These models are enhanced in [13, 14] to incorporate frequency support from both SG and CIGs. Moreover, to perform frequency-constrained energy management [16] utilises machine learning techniques to approximate the non-linear expressions of the frequency metrics resulting in a mixed-integer linear program. While the solution presented in [17, 18] proposes an iterative multi-stage approach that includes non-linear frequency constraints in a MG operational planning problem.

With respect to voltage security, in [19] the Differential-Algebraic-Discrete (DAD) equations describing the system dynamic response are discretized and applied to the security

dispatch problem to limit voltage dips and system instability. A sensitivity-based preventive control approach has been used in [20] to limit voltages within the secure loading margins in post-contingency states. Finally, in [21, 22], the transient voltage dynamics model is discretized and embedded into the reactive power planning problem to immunize against fault-induced delayed voltage recovery based on trajectory sensitivities.

The approaches proposed in the literature take two forms:

1) solving a single optimization problem with the inclusion of dynamic metrics based on analytical formulations or derived security indices [11–14]; and,

2) solving iterative multi-stage algorithms that feed information on the system's dynamic nature into the planning problem based on external analyses [17, 20, 23].

The latter group analyses the system dynamics separately and the results are used to formulate the constraints of the optimization problem. This approach benefits from a more accurate representation of the system through the use of the full non-linear dynamic model or time-domain simulations.

The up-to-now literature has focused on either optimising frequency response or voltage response. However, excursions stemming from abrupt MG islanding involve both voltage and frequency; thus, neglecting one can provide an optimistic evaluation of the MG security and resilience. In addition the above literature on optimising voltage security focuses on bulk transmission systems and looks into either long-term voltage stability margins [20, 22, 24] or the post fault transient voltage recovery [21] neglecting the effect of FRT limitations. The effect of dynamic frequency and voltage security during MG operational planning has not been adequately studied.

In this paper, we address these limitations by enhancing the MG operational planning problem while taking into account transient and static constraints relating to both voltage and frequency variations during and after an event-triggered emergency islanding. We include constraints on pre-contingency (grid-connected), post-contingency (islanded), and transient (switching) states of the MG, enabling both supply adequacy and the confinement of transient trajectories within secure regions. We enhance our work in [23] on secure voltage fault transients by adopting a dynamic optimisation technique, based on sequential constraint transcription, to represent both the voltage and frequency security constraints.

Consequently, the main contributions of this paper are:

- A multi-period, mixed-integer second-order cone MG operational planning problem that considers:
  - grid-connected and islanded mode of operation with security constraints on both the frequency and voltage transient performance during abrupt disconnection; and,
  - a hybrid MG with support offered by SGs, CIGs, and flexible loads in the preventive re-scheduling ensuring security during unscheduled islanding.

- A multi-stage solution algorithm that uses the sensitivities derived from dynamic simulations to formulate transient security constraints transcribed onto the MG operation problem through sequential resilience cuts.

(a)

(b)
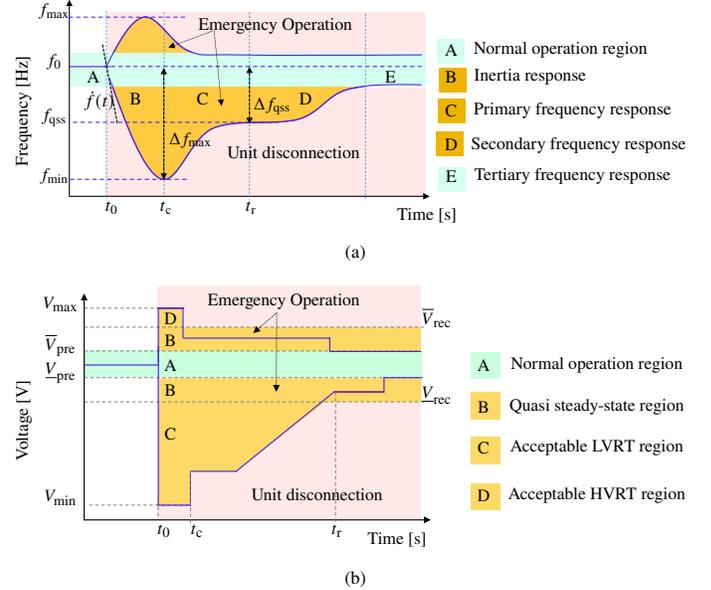
Fig. 1. DER frequency (a) and voltage (b) FRT profile and support regions with grid fault occurring at time t_0.

- A case study analysing the effect of both active and reactive power reserves on MG voltage and frequency security.

The rest of the paper is organized as follows. In Section II, the transient frequency and voltage metrics and the models adopted for MG support are presented. Section III presents the detailed problem formulation and proposed solution algorithm. Section IV discusses the application of the algorithm to a 30-bus test system to highlight the benefit of enhancing MG operational security and resilience. Finally, in Section V, the main conclusions of the paper are summarised.

II. FREQUENCY AND VOLTAGE SECURITY

A. Fault Ride-Through Criterion

Current grid codes are continually being modified with Fault Ride-Through (FRT) Requirements for Generators (RfG) to remain connected and supportive during transient grid faults [25]. For various levels of grid frequency and voltage drop/rise, the FRT RfG shows the time-frequency/time-voltage profiles for which the DERs should remain connected and support the grid by active/reactive power injection/absorption. The FRT is aimed at immunising against generation loss and where frequency or/and voltage support is provided to reduce the levels of degradation in the network. Figure 1 shows the profiles and support regions for frequency and voltage response after a major fault. Times t_0, t_c and t_r relate to time instance of fault occurrence, fault clearance and recovery period (quasi-steady-state), respectively. More precisely, time t_0 denotes the time of fault occurrence in the main grid resulting in the disconnection of the MG. This action is realised by opening the switch at the Point-of-Common-Coupling (PCC). Moreover, time t_c relates to the period within which the transient frequency and voltage excursions in the MG should be arrested and cleared after MG islanding i.e. the period between the start of a fault/contingency and

TABLE I
ENTSO-E RECOMMENDED PARAMETERS FOR FREQUENCY AND VOLTAGE
RIDE-THROUGH OF DERs WHERE $t_0 = 0$ s.

Frequency		Time [s]		Voltage [p.u]		Time [s]	
$\dot{f}(t)$	3 Hz/s	-	0.5				
$f_{\min}$	47.5 Hz	t_c	≤ 3	$V_{\min}$	0.4-0.5	t_c	≤ 0.2
$f_{\max}$	51.5 Hz	t_c	≤ 2	$V_{\max}$	1.2	t_c	≤ 0.2
$\underline{f}_{qss}$	49.8-49 Hz	t_r	≤ 4.5	$\underline{V}_{rec}$	0.7-0.9	t_r	≤ 2
$\overline{f}_{qss}$	50.2-51 Hz	t_r	≤ 2.5	$\overline{V}_{rec}$	1.1	t_r	≤ 2

the DER ceasing the provision of emergency support to the system. Furthermore, t_r defines the time following emergency disconnection within which the system should have re-gained a quasi-stable operating point.

In Fig. 1a the frequency deviation following a large disturbance is sketched highlighting the Inertial Response (IR) and Primary Frequency Response (PFR) regions for emergency frequency support. The main performance metrics used in resilience analysis include the maximum Rate-of-change of Frequency (RoCoF), $\left(\dot{f}(t)\right)$, the frequency nadir, $(\pm\Delta f_{max})$, and the post-fault steady-state frequency deviation, (Δf_{ss}).

Similarly, Fig. 1b shows the Low/High Voltage Ride-Through (L/HVRT) regions and the quasi-steady state regions for voltage support. The metrics for resilience analysis are defined by the security bounds on Low Voltage Ride-Through (LVRT), $V_{\min}$, High Voltage Ride-Through (HVRT), $V_{\max}$ and upper/lower post-fault recovery voltages, $\overline{V}_{rec}/\underline{V}_{rec}$. A unit will be tripped to avoid damage when these technical limits are exceeded, thus increasing the risk of further disconnections and cascading network failures.

Guidelines provided by the ENTSO-E for the FRT withstand capability requirements on frequency and voltage response are indicated in Table I [25]. In this work, we assume that the MG should be able to withstand the islanding transients at each planning instance $t \in \mathcal{T}$ without violating the FRT and L/HVRT criterion described in this section.

B. Frequency Support Model

Traditionally, only SG units were able to participate in all types of frequency support shown in Fig. 1a. These are equipped with a turbine/prime mover control and a governor that adjust the active power generation based on the measured frequency at the generator node [26]. However, CIGs with grid-supporting capabilities can now participate in frequency support even during the IR and PFR regions via techniques like synthetic inertia and droop control. Many control techniques have been proposed in the literature (e.g., [27, 28]) to increase/decrease power injection from CIGs during frequency events. In this work, for the CIGs, we adopt the Virtual Synchronous Machine (VSM) control framework in [29] for inertia emulation and a PFR support defined as:

$$p_{\mathrm{IR}}(t) = -K^{\mathrm{VSM}}\dot{f}_i(t) \tag{1a}$$

$$\Delta f(t) = f_i(t) - f_s(t) \tag{1b}$$

$$p_{\mathrm{PFR}}(t) = \begin{cases} 0, & \text{if } \underline{\Delta}f_{\mathrm{db}} < \Delta f(t) < \overline{\Delta}f_{\mathrm{db}} \\ -K^{\mathrm{D}}\Delta f(t), & \text{otherwise} \end{cases} \tag{1c}$$

$$p(t) = p_{\mathrm{pre}} + p_{\mathrm{PFR}}(t) + p_{\mathrm{IR}}(t) \tag{1d}$$

where K^{D} and K^{VSM} are the droop and synthetic-inertia constants, respectively; f_i and f_s are the frequency measured at the local converter node and synchronous frequency, respectively; the lower and upper frequency dead band region where no PFR support is applied is given by $\underline{\Delta}f_{\mathrm{db}}$ and $\overline{\Delta}f_{\mathrm{db}}$, respectively; p_{pre} is pre-fault active power generation set-point of the unit; and, $p(t)$ is the transient active power generation reference for the CIG that includes frequency support. For the SG units, the 'DEGOV' diesel engine turbine-governor model [30] is adopted in this work.

C. Voltage Support Model

The momentary injection or absorption of reactive power during the period of voltage degradation or rise has been shown to provide support to ensure system integrity is protected [31, 32]. The CIG control framework provides dynamic voltage support by prioritising reactive power injection (during voltage drop) and absorption (during voltage rise) outside of the normal operating limits (see the emergency operation in Fig. 1b) as indicated in (2) [31].

$$q(t) = q_{\mathrm{pre}} + \begin{cases} K^{\mathrm{I}} \cdot i_{\mathrm{Q,max}} \cdot (\underline{V}_{\mathrm{pre}} - V(t)) & \text{if } V(t) < \underline{V}_{\mathrm{pre}} \\ K^{\mathrm{A}} \cdot i_{\mathrm{Q,max}} \cdot (\overline{V}_{\mathrm{pre}} - V(t)) & \text{if } V(t) > \overline{V}_{\mathrm{pre}} \\ 0 & \text{otherwise} \end{cases} \tag{2}$$

The pre-fault reactive power generated by the CIG is denoted by q_{pre} and parameters K^{I} and K^{A} define the respective rate of change of reactive power with respect to a change in voltage. The reactive power reference provided to the unit is defined by $q(t)$.

The support offered by the CIG unit depends on the maximum available active and reactive power. This output is limited by the nominal current rating, i_{nom}, of the CIG and subject to the dynamic security thresholds. During dynamic voltage support, the unit prioritises reactive current injection over active current. It is however necessary that the nominal current limits are not exceeded. This is ensured by a limit updating current priority logic described as:

$$i_{\mathrm{P,max}} = F_{\mathrm{PQ}}i_{\mathrm{nom}} + (1 - F_{\mathrm{PQ}})\sqrt{i_{\mathrm{nom}}^2 - i_{\mathrm{Q}}^2}$$
$$i_{\mathrm{Q,max}} = F_{\mathrm{PQ}}\sqrt{i_{\mathrm{nom}}^2 - i_{\mathrm{P}}^2} + (1 - F_{\mathrm{PQ}})i_{\mathrm{nom}} \tag{3}$$

where binary flag (0/1) F_{PQ} is used to indicate whether active or reactive current injection has priority i.e., F_{PQ} is set to 0 when dynamic voltage support is required thereby giving priority to reactive current for voltage support. The reference active and reactive currents i_{P} and i_{Q}, respectively provided for the converter output are thus limited based on the setting of $i_{\mathrm{P,max}}$ and $i_{\mathrm{Q,max}}$.

Evidently, voltage support in conventional SGs is ensured by the over/under excitation limiters. The excitation system can rapidly vary the field current and voltage in response to the disturbances in the network. The IEEE AC1A [33] excitation model is adopted for voltage support by the SGs.

III. MG PLANNING PROBLEM FORMULATION

A. Preliminaries

Bold letters are used to indicate vectors while entries of vectors are denoted by regular letters. Cardinallity of the previously defined sets is denoted by: $n_d := |\mathcal{D}|$, $n_s := |\mathcal{S}|$, $n_l := |\mathcal{L}|$, and $n_c := |\mathcal{C}|$, respectively. Indices s, c and d are associated with synchronous generators, RESs and load demand while index $g \in \mathcal{M}$ is associated with all generating units. The main modeling preliminaries in the proposed operational planning model are:

- This work considers a radial three-phase balanced network represented by a connected graph $\mathcal{G}(\mathcal{N}, \mathcal{L})$. The interface between the MG and the bulk grid is located at the PCC. The power flow is modelled using an extended version of the DistFlow model [31] to include the shunt line parameters.
  While distribution networks are inherently unbalanced, the adoption of the balanced model reduces the computational complexity of the dynamically-constrained planning problem proposed. It is possible to extend the methodology for incorporating the unbalanced behaviour of three-phase MGs by extending both the power-flow formulation, the dynamic modelling, and the constraints to the three-phase unbalanced counterparts. However, both the modelling requirements and the computational complexity would render the methodology impractical for long planning horizons and large MGs.
- For the proposed MG planning algorithm, the optimization problem is formulated to include three sets of operational constraints relating to pre-emergency steady-state operation (grid-connected mode); post-emergency steady-state operation (islanded mode); and transient state operation (islanding mode).
- The problem formulation for grid-connected operation is defined over a planning horizon $\mathcal{T}$ where $|\mathcal{T}| = 24$ hours. Without loss of generality, we consider hourly planning periods.
- For each hour $t \in \mathcal{T}$, a potential emergency islanding event in the MG is assumed. Once the MG is islanded, only one hour of islanded operation is taken into account. Moreover, the probability of further contingencies in the islanded mode is not considered.
- The cause of microgrid islanding is a major fault in the external main grid network resulting in the emergency disconnection of the MG from the main grid.
- Further measures to re-synchronise the MG with the main grid within or after the one-hour emergency operation given the fault in the main grid has been cleared are not explicitly handled in this paper.

B. Formulation of the Dynamically-Constrained Planning Problem

The response of the system in the event of large disturbances, such as fault-triggered islanding, is governed by the behaviour of the loads, generators, and network, described by differential-algebraic equations. In addition, a change in control configuration can be triggered based on a measured value of a system state. This operation adds discrete states to the existing continuous states resulting in a system governed by a set of Differential-Algebraic and Discrete (DAD) equations. The model of a dynamically constrained planning problem can be represented as shown in (4).

$$\min_{\boldsymbol{u}} f(\boldsymbol{y}, \boldsymbol{u}) \tag{4a}$$

s.t.

$$\boldsymbol{g}(\boldsymbol{y}, \boldsymbol{u}) = \boldsymbol{0} \tag{4b}$$

$$\boldsymbol{h}(\boldsymbol{y}, \boldsymbol{u}) \leq \boldsymbol{0} \tag{4c}$$

$$\boldsymbol{m}(\dot{\boldsymbol{x}}, \boldsymbol{x}, \boldsymbol{y}, \boldsymbol{u}) = \boldsymbol{0} \tag{4d}$$

$$\boldsymbol{n}(\boldsymbol{x}, \boldsymbol{y}, \boldsymbol{u}) \leq \boldsymbol{0} \tag{4e}$$

$$\underline{\boldsymbol{y}} \leq \boldsymbol{y} \leq \overline{\boldsymbol{y}}, \quad \underline{\boldsymbol{x}} \leq \boldsymbol{x} \leq \overline{\boldsymbol{x}}, \quad \underline{\boldsymbol{u}} \leq \boldsymbol{u} \leq \overline{\boldsymbol{u}} \tag{4f}$$

where $\boldsymbol{y}$ represents the steady-state operational variables (nodal voltages, power flows in the distribution lines and power consumption by load in the network) while $\boldsymbol{u}$ denote the control variables, these include the active and reactive power injections by the different generation units and the power exchange with the grid. Equation (4b) corresponds to the AC power flow network constraints in steady-state operation, while (4c) includes the different techno-economic operational constraints applied to the network such as line loading constraints, voltage constraints and generation limits on the different units. The system dynamics after MG islanding are represented by the set of differential-algebraic equations in (4d), where variables $\boldsymbol{x}$ denote the differential state variables. The transient response trajectory constraints (see Fig. 1) are defined in (4e), while (4f) ensure the security bounds on variables. The goal is to find optimal values of the control variables $\boldsymbol{u}^*$ such that the cost function (4a) is minimised, all constraints are satisfied, and that will drive the system response to a feasible post-islanding transient trajectory $\boldsymbol{x}^*$.

The problem in (4) is however difficult to solve due to its infinite dimensions and highly nonlinear nature [34]. It includes a system of both analytical and differential equations defined for every unit at each node in the network and for every period in the planning horizon. Moreover, any discrete control states add a further dimension to the solution space. The optimal solution to (4) should satisfy the dynamics of the system, the path constraints on system variables as well as the network power flow equations. However, such a problem is too complex to be solved by off-the-shelf solvers.

Different approaches have therefore been proposed in power systems to solve problems with a similar structure as (4), including dynamic optimisation techniques, analytical methods based on the Single-Machine Equivalent (SME), and computational intelligence methods such as machine learning techniques [35–37]. Obtaining a true analytical solution to the closed-form model describing the system dynamic response using the SME method is not a straightforward operation when considering both voltage and frequency response in the network. Especially with regards to CIG-dominated networks that adopt a discrete control support mechanism, as described in (1) and (2). Moreover, unit saturation and limit cycles that can occur especially during emergency states can result in further modelling complexities.

On the other hand, full discretization of (4d)-(4e) by embedding numerical integration methods, as described in [19], ensures that steady-state and dynamic equations are simultaneously satisfied. However, each step of the discretization introduces a new set of optimization states with inter-temporal coupling between them. It is quite evident that this process can quickly expand the solution space of the optimization problem making it intractable.

Finally, the direct sequential method adopted in this paper is a technique for solving dynamically constrained problems where only the control states are discretized and approximated based on a basis function in each section of the discretized time window [35]. The basis functions at each time stage can be piece-wise constant, linear, quadratic, or polynomial functions [34]. This allows for the decoupling of the model (4) where the control variables can be estimated in the time-domain simulation of the DAD model (4d)-(4e) and trajectories of the state variables in the optimization problem estimated based on their gradients w.r.t the control variables in the time-domain simulation.

In this work, we use piece-wise constant functions to approximate control variables. Thus, the control variables vector $\boldsymbol{u}$ is approximated as:

$$\boldsymbol{u} = \boldsymbol{u}_k, \qquad k = 1, \ldots, n \tag{5}$$

where k is the iterative stage. At the same time, the performance metrics $\boldsymbol{\mu}$, described in Section II-A, can be approximated as:

$$\boldsymbol{\mu}_k = \boldsymbol{\mu}_{k-1} + \boldsymbol{\delta}_{\mu,k}^u (\boldsymbol{u}_k - \boldsymbol{u}_{k-1}), \qquad k = 1, \ldots, n \tag{6}$$

where $\delta_{\mu,k}^u$ is the gradient (i.e. sensitivity) of the performance metric μ w.r.t the control variable u at iteration k.

Therefore, (6) replaces (4d)-(4e) transforming the model (4) for the k-th iteration to:

$$\min_{\boldsymbol{u}_k} f(\boldsymbol{y}_k, \boldsymbol{u}_k) \tag{7a}$$

s.t.

$$\boldsymbol{g}(\boldsymbol{y}_k, \boldsymbol{u}_k) = \boldsymbol{0} \tag{7b}$$

$$\boldsymbol{h}(\boldsymbol{y}_k, \boldsymbol{u}_k) \leq \boldsymbol{0} \tag{7c}$$

$$\boldsymbol{\mu}_k = \boldsymbol{\mu}_{k-1} + \boldsymbol{\delta}_{\mu,k}^u (\boldsymbol{u}_k - \boldsymbol{u}_{k-1}) \tag{7d}$$

$$\underline{\boldsymbol{y}} \leq \boldsymbol{y}_k \leq \overline{\boldsymbol{y}}, \quad \underline{\boldsymbol{\mu}} \leq \boldsymbol{\mu}_k \leq \overline{\boldsymbol{\mu}}, \quad \underline{\boldsymbol{u}} \leq \boldsymbol{u}_k \leq \overline{\boldsymbol{u}} \tag{7e}$$

where the time-domain-related variables and constraints have been replaced by the performance metrics extracted from the time-domain simulations.

The resulting problem in (7) is a finite-dimensional problem that can be easily solved by off-the-shelf optimization tools. Using the direct sequential method, an iteration between the optimization problem and a time-domain simulation continues until both optimality and feasibility, based on the defined stopping criteria, are obtained.

C. Design of the Transient Security Constraints

In this paper, the performance metrics $\boldsymbol{\mu}$ of concern are defined in Fig. 1, relating to the values of frequency and voltages during the emergency response of the different generation units. The control states relate to the active and reactive power

injections of both the grid and the DERs prior to emergency islanding. Therefore at each iteration, the path constraints in (7d) take the form:

1) Frequency Transient Constraints: We utilise the CoI frequency response to model the frequency transient response. While the CoI model shows slight variations as compared to the local frequency oscillations of the generating units, it provides a smoother overall frequency that aids the provision of better control from CIGs [38, 39]. The path constraints on frequency response from (7d)-(7e) at the k-th iteration take the form:

$$\boldsymbol{\omega}_{(k+1)}^{cr} \leq \boldsymbol{\omega}_\gamma^{cr} + \boldsymbol{\delta}_{\omega^{cr},\gamma}^{p^{grid}} \cdot (\boldsymbol{p}_{(k+1)}^{grid} - \boldsymbol{p}_\gamma^{grid})$$
$$+ \boldsymbol{\delta}_{\omega^{cr},\gamma}^{q^{grid}} \cdot (\boldsymbol{q}_{(k+1)}^{grid} - \boldsymbol{q}_\gamma^{grid}) + \Delta\boldsymbol{\omega}_{slk}^{cr}, \ \forall\gamma = 1, \ldots, k \tag{8a}$$

$$\omega_{k+1}^{min} \geq \underline{\omega}^{min}, \qquad \omega_{k+1}^{max} \leq \overline{\omega}^{max} \tag{8b}$$

$$\underline{\dot{\omega}} \leq \dot{\omega}_{k+1} \leq \overline{\dot{\omega}} \tag{8c}$$

$$\underline{\omega}^{qss} \leq \omega_{k+1}^{qss} \leq \overline{\omega}^{qss} \tag{8d}$$

where superscript $^{cr} \in \{\mathrm{RoCoF, min, max, qss}\}$ correspond to the magnitudes of RoCoF, frequency nadir, frequency zenith and quasi-steady state frequency, respectively. $\Delta\omega_{slk}^{cr}$ is a slack variable added to prevent infeasibility of the problem.

The controlled states (u) considered in this work are the active and reactive power injections by the different generation units ($\boldsymbol{p}_g$ and $\boldsymbol{q}_g$) and the power exchange with the grid (p^{grid} and q^{grid}). However, in reality, the second set of decision variables is a function of the first set, through the DistFlow equations. Therefore, for the frequency response, the control variables are defined by active (p^{grid}) and reactive (q^{grid}) power exported or imported from the grid at each hour prior to emergency islanding.

Constraints (8b)-(8d) are applied to restrict the frequency states within the technical boundaries illustrated in Fig. 1 where units remain connected to the network.

It is noteworthy to mention that in (8a) the equality sign has been replaced with an inequality, ensuring the satisfaction of the path constraint at all previous iterations. This transformation adds multiple constraints with the aim of tightening the feasible state space and restricting trajectories within the secure regions defined in Fig. 1. It also enhances the convergence rate of the solution algorithm. In case an equality sign is adopted in (8a), a single constraint is considered at each iteration. The history and effect of previous operating points are not taken into account. This can present the risk of the algorithm entering an infinite iterative loop that can result in non-convergence of the algorithm. Moreover, a lack of sensitivity information from previous iterations can easily provide a non-optimal but feasible solution.

2) Voltage Transient Constraints: Due to the very local nature of voltage evolution, the transient voltage metrics are formulated at the terminal node of each generator unit. For generator $g \in \{\mathcal{S}, \mathcal{C}\}$, the transient voltage constraints are formulated as:

$$\boldsymbol{V}_{(k+1)}^{cr} \leq \boldsymbol{V}_\gamma^{cr} + \sum_{g \in \{\mathcal{S},\mathcal{C}\}} \left(\boldsymbol{\delta}_{V_g^{cr},\gamma}^{p_g} \cdot (\boldsymbol{p}_{g,(k+1)} - \boldsymbol{p}_{g,\gamma}) \right.$$
$$\left. + \boldsymbol{\delta}_{V_g^{cr},\gamma}^{q_g} \cdot (\boldsymbol{q}_{g,(k+1)} - \boldsymbol{q}_{g,\gamma}) \right) + \Delta\boldsymbol{V}_{slk}^{cr}, \ \forall\gamma = 1, \ldots, k \tag{9a}$$

$$V_{k+1}^{\text{LVRT}} \geq \underline{V}_{\min}, \qquad V_{k+1}^{\text{HVRT}} \leq \overline{V}_{\max} \qquad (9b)$$

$$\underline{V}_{\text{rec}} \leq V_{k+1}^{\text{rec}} \leq \overline{V}_{\text{rec}} \qquad (9c)$$

where superscript $^{\text{cr}} \in \{\text{LVRT, HVRT, rec}\}$ correspond to the voltage magnitudes at LVRT, HVRT and post-fault recovery voltage, respectively. For the voltage resilience metrics in (9a), the effect of the post-emergency voltage levels at the terminals of each generator on the pre-emergency active and reactive power injections at all generators in the network is considered when formulating the linearized path constraint. Hence, the control states are characterised by active (p_g) and reactive (q_g) power injected by all generators. The slack variable $\Delta V_{\text{slk}}^{\text{cr}}$ immunises against infeasibility of the problem while constraints (9b)-(9c) ensure voltages at each generator are not in the region where unit disconnection occurs. The use of the slack variables is vital given the high probability of conflicting constraints when both frequency and voltage constraints are applied. These are heavily penalised in the objective function.

Constraints (8) and (9) define the transient islanding constraints applied at each hour of the planning horizon. These ensure system states are maintained within the acceptable emergency operation regions illustrated in Fig. 1.

D. Static Operation Constraints

The steady-state operation constraints are designed to provide a snapshot of system performance at each hour of the planning horizon. These include constraints on the grid-connected and islanded operation of the MG associated to (7b)-(7c) and defined in extended form as:

1) Constraints on Power Flow and Power Balance: The constraints on active and reactive power flows in the network have been formulated using a Second-Order Cone Programming (SOCP) model defined in [40], which extends the DistFlow power model to include the line charging:

$$s_{it} = \sum_{d \in \mathcal{D}^i} s_{dt} - s_{t|i=\text{PCC}}^{\text{imp}} + s_{t|i=\text{PCC}}^{\text{exp}} \qquad (10a)$$

$$\qquad - \sum_{g \in \{\mathcal{S}^i, \mathcal{C}^i\}} s_{gt}, \qquad \forall i \in \mathcal{N}, \ t \in \mathcal{T}$$

$$s_{it} = \sum_{\eta(l^+)=i} S_{l+} + \sum_{\eta(l^-)=i} S_{l-} \qquad \forall i \in \mathcal{N}, \ t \in \mathcal{T} \quad (10b)$$

$$f_{tl+} v_{t\eta(l+)} \geq |S_{tl+}|^2 \text{ or } f_{tl-} v_{t\eta(l-)} \geq |S_{tl-}|^2, \qquad (10c)$$
$$\forall l \in \mathcal{L}, \ t \in \mathcal{T}$$

$$|\alpha_{l+}|^2 v_{t\eta(l+)} - v_{t\eta(l-)} = 2\,\text{Re}(\alpha_{l+} z_l^* S_{tl+}) - |z_l|^2 f_{tl+}, \qquad (10d)$$
$$\forall l \in \mathcal{L}, \ t \in \mathcal{T}$$

$$|\alpha_{l-}|^2 v_{t\eta(l-)} - v_{t\eta(l+)} = 2\,\text{Re}(\alpha_{l-} z_l^* S_{tl-}) - |z_l|^2 f_{tl-}, \qquad (10e)$$
$$\forall l \in \mathcal{L}, \ t \in \mathcal{T}$$

$$\alpha_{l+}^* v_{t\eta(l+)} - z_l^* S_{tl+} = \left(\alpha_{l-}^* v_{t\eta(l-)} - z_l^* S_{tl-}\right)^*, \qquad (10f)$$
$$\forall l \in \mathcal{L}, \ t \in \mathcal{T}$$

Constraint (10a) ensures the power balance at each node. Note that power import/export from the grid is only defined at the PCC node. In islanded mode, the power import and export to the grid are set to zero. Equations (10b)-(10f) describe the

power flow equations with parameter $\alpha_{l+} = 1 + z_l y_{l+}^{sh}$. The equality in constraint (10c) has been relaxed to an inequality to transform the power flow equation from a non-linear to SOCP model to improve tractability and global optimality.

2) Constraints on Grid Power Exchange: Defined only for the grid-connected mode, the bounds on power imports and exports to the grid take the form:

$$0 \leq p_t^{\text{imp}} \leq \overline{p}_t^{\text{imp}} \cdot z_t^{\text{P}}, \quad 0 \leq p_t^{\text{exp}} \leq \overline{p}_t^{\text{exp}} \cdot (1 - z_t^{\text{P}}),$$
$$0 \leq q_t^{\text{imp}} \leq \overline{q}_t^{\text{imp}} \cdot z_t^{\text{Q}}, \quad 0 \leq q_t^{\text{exp}} \leq \overline{q}_t^{\text{exp}} \cdot (1 - z_t^{\text{Q}}), \quad \forall t \in \mathcal{T}$$
$$(11)$$

where the binary variables $z_t^{\text{P}}/z_t^{\text{Q}}$ prevent the simultaneous import and export of active/reactive power.

3) Constraints on Loads: Power consumption of load at each node can be fixed (s_{dt}^{f}) or variable (s_{dt}^{v}) i.e. flexible load, the limitations applied to the load variations over the planning horizon include:

$$[p/q]_{dt} = ([p/q]_{dt}^{\text{f}} + [p/q]_{dt}^{\text{v}}) \cdot z_{dt}, \qquad \forall d \in \mathcal{D}, \ t \in \mathcal{T} \quad (12a)$$

$$0 \leq p_{dt} \leq \overline{p}_d, \quad 0 \leq q_{dt} \leq \overline{q}_d, \qquad \forall d \in \mathcal{D}, \ t \in \mathcal{T} \quad (12b)$$

$$\sum_{t \in \mathcal{T}} p_{dt}^{\text{d}} = E_d, \qquad \forall d \in \mathcal{D} \quad (12c)$$

$$p_{dt} \leq E_d - \sum_{\tau=1}^{t-1} p_{d\tau}, \qquad \forall d \in \mathcal{D}, \ t \in \mathcal{T} \quad (12d)$$

where the binary variable z_{dt} indicates the connection status of the load. In grid connected mode, this value is forced to one i.e. all load should be served in its entirety. On the contrary, in islanded mode, z_{dt} can take on a value of one $\implies$ load-connected or zero $\implies$ load-curtailed. Constraint (12b) ensures the total load does not exceed the peak load defined at a given node, this is defined based on the maximum consumption at a node. Note that flexible loads relate to large consumers that are able to upwardly/downwardly adjust consumption when required within their maximum consumption limits. In grid connected mode, constraint (12c) ensures that the defined energy consumption E_d for the day is met. During islanded operation, (12d) ensures that only un-served load consumption is met. The fraction of un-served load at any hour given the daily requirement is defined by the right-hand side of (12d).

4) Constraints on power production from SGs:

$$0 \leq p_{st} + p_{st}^{\text{FR}} \leq \overline{p}_s, \qquad \forall s \in \mathcal{S}, t \in \mathcal{T} \quad (13a)$$

$$\underline{q}_s \leq q_{st} \leq \overline{q}_s, \qquad \forall s \in \mathcal{S}, t \in \mathcal{T} \quad (13b)$$

$$p_{st}^{\text{FR}} \cdot \Delta t \leq E_s^{\text{FR,max}} \qquad \forall s \in \mathcal{S}, t \in \mathcal{T} \quad (13c)$$

$$-rd_s \leq p_{st} - p_{s(t-1)} \leq ru_s, \qquad \forall s \in \mathcal{S}, t \in \mathcal{T} \quad (13d)$$

The limits to power output of the SG units are defined in (13a)-(13b) where p_{st}^{FR} defines the power reserve capacity of each generator allocated to transient frequency control. Constraint (13c) ensures that energy reserves availed to frequency support are within the maximum limit $E_s^{\text{FR,max}}$ that the unit can provide. Here, parameter Δt is the response duration for frequency support. The energy limit is defined based on the nominal capacity of the generator. The inter-hour ramp-up ru_s and ramp-down rd_s limits of the SG units are ensured in (13d).

5) Constraints on power production from CIGs: In line with the current grid code, the operation of renewable energy units at a power factor less than one is allowed, thus the limits on power production from CIG units are defined as:

$$0 \le p_{ct} + p_{st}^{\text{FR}} \le \overline{p}_{ct}, \qquad \forall c \in \mathcal{C}, t \in \mathcal{T}, \qquad (14a)$$

$$0 \le q_{ct} \le \tan(\overline{\phi}) \cdot \overline{p}_{ct}, \qquad \forall c \in \mathcal{C}, t \in \mathcal{T}, \qquad (14b)$$

$$p_{ct}^{\text{FR}} \cdot \Delta t \le E_c^{\text{FR,max}} \qquad \forall c \in \mathcal{C}, t \in \mathcal{T} \qquad (14c)$$

where $\cos(\overline{\phi})$ is the minimum acceptable power factor of the CIG defined by the grid code. The active and reactive power limits are defined in (14a) and (14b), respectively. The limitation adopted in (14b) is flexible as it allows for reactive power generation at the maximum level, $\overline{q}_{ct}$, even at instances with low active power injection [41]. Constraint (14c) limits the energy reserves offered by the CIG unit to the maximum limit $E_c^{\text{FR,max}}$.

6) Constraints on Steady-Stage Voltage: Voltage levels at each node in steady-state operation should be maintained within the normal operation region illustrated in Fig. 1b. In both grid-connected and islanded mode, this is ensured by:

$$\underline{v} \le v_{it} \le \overline{v}, \quad v_{t|i=\text{PCC}} = 1 \text{ pu}, \qquad \forall i \in \mathcal{N}, \ t \in \mathcal{T} \quad (15)$$

In grid-connected mode, the voltage at the PCC is maintained by the stiff grid. However, during islanded mode voltage is controlled by the DERs present in the network. This can be realised using a single-master or with a multi-master operating mode [42]. In this paper, the largest SG unit in the network provides the voltage reference when the power supply to/from the grid is lost. Moreover, the CIG units provide further voltage and reactive power support based on (14b).

7) Constraints on Line Loading: The transmission capacity of each line is maintained within secure bounds as:

$$0 \le f_{tl+} \le (\overline{f}_l), \quad 0 \le f_{tl-} \le (\overline{f}_l), \quad \forall l \in \mathcal{L}, \ t \in \mathcal{T} \quad (16)$$

8) Objective Function: The objective is a min-max function that contains a minimization of the grid-connected mode operational costs, $\Theta^{\text{gm}}(\boldsymbol{y}^{\text{gm}})$ under the worst case islanding penalties at each hour $\Theta_t^{\text{im}}(\boldsymbol{y}^{\text{im}})$ defined as a single minimization problem by utilizing auxiliary variable α:

$$\min_{\boldsymbol{y}} \ \Theta^{\text{gm}}(\boldsymbol{y}^{\text{gm}}) + \alpha \qquad (17a)$$

s.t.

$$\alpha \ge \Theta_t^{\text{im}}(\boldsymbol{y}^{\text{im}}), \qquad \forall t \in \mathcal{T}, \qquad (17b)$$

$$\begin{aligned}
\Theta^{\text{gm}}(\boldsymbol{y}^{\text{gm}}) = \sum_{t \in \mathcal{T}} &\bigg(\left(C^{\text{imp}^{\text{P}}} \cdot p_t^{\text{imp}} - C^{\text{exp}^{\text{P}}} \cdot p_t^{\text{exp}} \right) \\
&+ \left(C^{\text{imp}^{\text{Q}}} \cdot q_t^{\text{imp}} - C^{\text{exp}^{\text{Q}}} \cdot q_t^{\text{exp}} \right) \bigg) \\
&+ \sum_{t \in \mathcal{T}} \sum_{g \in \{\mathcal{S}, \mathcal{C}\}} \left(C_g^{\text{P}} \cdot p_{gt} + C_g^{\text{Q}} \cdot q_{gt} \right) + \sum_{t \in \mathcal{T}} \sum_{d \in \mathcal{D}^{\text{v}}} \left(C_d^{\text{v}} \cdot p_{dt}^{\text{v}} \right) \\
&+ \sum_{t \in \mathcal{T}} \sum_{\text{cr} \in \text{cr}^{\text{CoI}}} \left(C_{\text{slk}}^{\text{cr}} \cdot \Delta \omega_{\text{slk},t}^{\text{cr}} \right) \\
&+ \sum_{t \in \mathcal{T}} \sum_{g \in \{\mathcal{S}, \mathcal{C}\}} \sum_{\text{cr} \in \text{cr}^{\text{V}}} \left(C_{\text{slk}}^{\text{cr}} \cdot \Delta V_{\text{slk},g,t}^{\text{cr}} \right)
\end{aligned}$$
$$(17c)$$
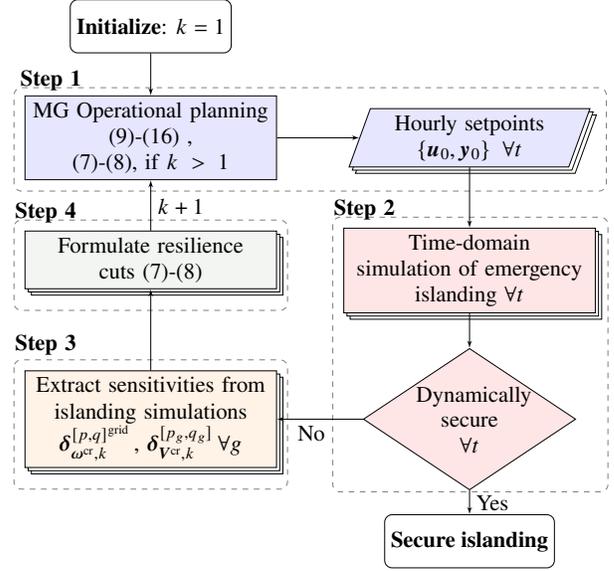
Fig. 2. Proposed Solution Algorithm

$$\Theta_t^{\text{im}}(\boldsymbol{y}^{\text{im}}) = \sum_{d \in \mathcal{D}} \left(C_d \cdot (1 - z_{dt}) \left(p_{dt}^{\text{f}} + p_{dt}^{\text{v}} \right) \right) \qquad (17d)$$

In grid connected mode, (17c), the active/reactive power is imported/exported from/to the grid at costs $C^{\text{imp}^{\text{P/Q}}}/C^{\text{exp}^{\text{P/Q}}}$ while the generation costs of the different generators are defined by $C_g^{\text{P/Q}}$. Additionally, penalty costs C_d^{v} applied to the variable loads due the inconvenience of shifting demand away from the consumer preferred time. High penalty costs $C^{\text{CoI,slk}}$ and $C_g^{\text{cr,V}}$ are applied to the slack variables to ensure they are only utilised when absolutely necessary. The islanded operation costs in (17d) denote the penalties C_d incurred when a load is curtailed during the emergency operation. The overall optimization problem is formulated as a Mixed-Integer Second-Order Cone Programming (MISOCP) problem.

E. Solution Algorithm

The proposed solution approach iterates between an optimisation problem, a time-domain dynamic simulation, and an extraction stage as illustrated in Fig. 2. The tasks involved in each step are detailed as follows:

Step 1: Initially, setting iteration $k = 1$, the grid-connected and islanded mode MG scheduling problems, i.e. (10)-(17), are solved simultaneously to derive the output vectors $\boldsymbol{u}_{0,t}, \boldsymbol{y}_{0,t}$ of the optimised hourly operating points. Subscript $_0$ is used to indicate the pre-contingency steady state (see Fig. 1) value of the respective control and state variables. The grid-connected mode problem is solved for the entire planning horizon $\mathcal{T}$ together, while a one-hour islanded operation problem is solved at each hour $t \in \mathcal{T}$. The optimisation problem (10)-(17) ensures both static security and system adequacy in the pre- and post-islanded MG operation. The problem is robust to abrupt islanding at each hour defined by the loss of power from the grid.

Step 2: In this step, the hourly operating points in grid-connected mode from Step 1 are used to perform time-domain dynamic simulations considering abrupt islanding. These are

performed to check that voltage and frequency trajectories remain within the secure regions based on the metrics defined in Section II-A. If all performance metrics are satisfied, secure islanding is assumed. Otherwise, the algorithm formulates resilience cuts in Steps 3 and 4 to be added to the scheduling problem of Step 1.

Step 3: The value of each metric is derived from the measurements of the frequency and voltage states between times t_0 to t_r (see Fig. 1) during the MG transition to the islanded state. Given any security violations at any hour of the planning horizon, the sensitivity coefficients ($\delta_{\omega^{cr},k}^{[P,Q]^{grid}}$ and $\delta_{V^{cr},k}^{[P_g,Q_g]}$) of the frequency and voltage metrics to the respective control states (power injections) are obtained. In this paper, the finite difference method is used to calculate the sensitivities. This is based on multiple time-domain simulations of the emergency disconnections with variations of active or reactive power for each control variable in the pre-contingency steady-state.

Step 4: The feasibility resilience cuts at iteration k defined in (8)-(9) are formulated for each hour based on the values of the metrics and associated sensitivities. These are then applied to the grid-connected optimisation problem in Step 1. The problem in Step 1 is updated and re-solved including all resilience cuts from $\gamma = 1$ to k.

IV. SIMULATION RESULTS

A. System Setup

The proposed algorithm was evaluated on a 30-bus, 20 kV, distribution network shown in Fig. 3 with three CIGs and two SG units and base power of 10 MVA. The network topology and line parameters were obtained from [43]. It serves 12 loads modelled as constant current for active power and constant impedance for reactive power, in addition to three induction motors at buses 14, 20 and 28. In the steady-state optimization problem, all loads are modelled as constant power loads with peak load consumption at 15 MVA. The CIGs are modelled based on reference [31] with added VSM
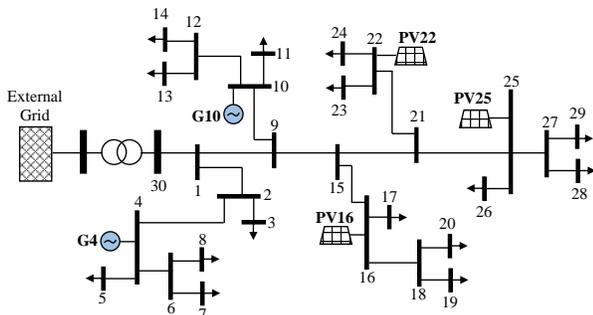
Fig. 3. One-line diagram of test system.
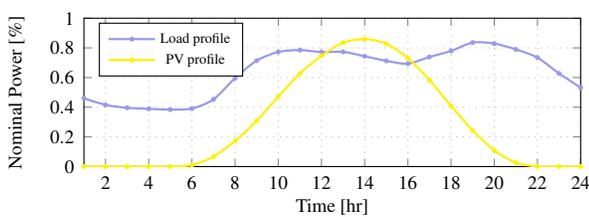
Fig. 4. Solar power generation and load demand profiles.

control for frequency support as in (1). For the SGs, a 6th-order model equipped with the DEGOV1 speed governor and the IEEE AC1A exciter is adopted. The dynamic simulation was performed with PyRAMSES [44], while the optimization model was implemented in PYOMO [45] and GUROBI [46] employed as a solver. The load and solar profiles (shown in Fig. 4) are adopted from [47] and power import, export, and SG production costs were set to 15 \$/MW, 5 \$/MW and 40 \$/MW, respectively.

The dynamic response during emergency islanding is simulated after a three phase fault at the high-voltage bus occurring at $t_0 = 1$ s, the fault is cleared by performing an emergency islanding of the MG after five cycles. Maximum clearing time t_c is set at 0.5 s for voltage transients and 2 s for frequency transients while maximum t_r is set at 1.5 s for voltage and 4 s for frequency (see Fig. 1). The MG performs an emergency islanding five cycles after clearing the fault by opening the interconnection at the PCC (node 30). From Fig. 1, the limits to the performance metrics have been set as: $\dot{f}(t) = \pm 3$ Hz/s, $f_{max} = 50.8$ Hz, $f_{min} = 49.6$ Hz, $f_{qss} = 49.8/50.2$ Hz, for the frequency response and $V_{min} = 0.45$ p.u., and $V_{max} = 1.2$ p.u., $\underline{V}_{rec} = 0.9$ p.u. and $\overline{V}_{rec} = 1.1$ p.u. for the voltage trajectories. The steady-state voltages in normal operation are set within bounds of $\underline{V}_{pre} = 0.95$ p.u. to $\overline{V}_{pre} = 1.05$ p.u.

To investigate the effect of transient-aware MG scheduling on system security, we consider three different cases in the operational planning problem:

- Base case: No transient security constraints. Only MG static islanding constraints
- Case 1: The constraints of the Base case plus transient frequency security constraints
- Case 2: The constraints of the Base case plus transient voltage security constraints
- Case 3: The constraints of the Base case plus both transient frequency and voltage security constraints.

B. Preventive Power Rescheduling

Cases 1, 2 and 3 result in both active and reactive power rescheduling to ensure the satisfaction of the transient security requirements. Figure 5 shows the scheduled power exchange with the grid for each of the cases. In Case 1 (see Fig. 5-green), the active power imported from the grid is shown to significantly reduce at hours 10, 19, 20, and 21 compared to the Base Case. This is a result of the actions taken to ensure the secure frequency transient response in case of unplanned islanding. However, the effect on reactive power is less substantial. An average hourly power increase of 0.062 MVar is recorded for reactive power in comparison to an average reduction of 0.521 MW in the case of active power for the entire planning horizon compared to the Base case. As expected, the sensitivities of active power to the frequency metrics are more significant than those to reactive power. The reduction in active power imported from the grid implies that more power has to be generated locally in the MG to improve the system frequency response in the case of unintentional islanding.
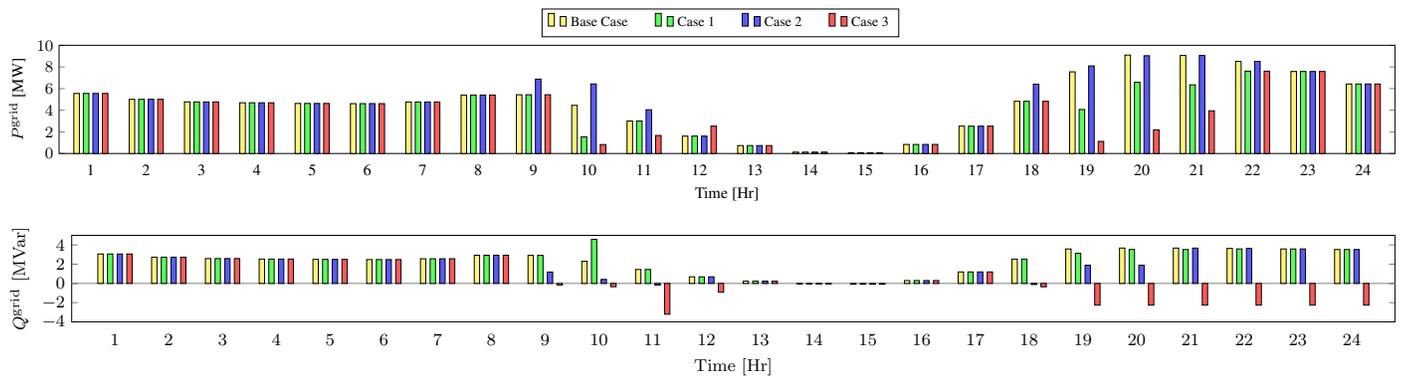
Fig. 5. Scheduling of active and reactive power exchanged with the grid for the different planning cases ((+) indicates power import and (-) indicates power export).

With only voltage transient security considered in Case 2 (see Fig. 5-blue), an average hourly active power increase of 0.272 MW and a reactive power reduction of 0.473 MVar is observed compared to the Base case. Local reserves of reactive power are used to ensure non-violation of the voltage security metrics during islanding. Note that these are mainly provided by the SG units as the system will prioritise the cheap active power from the renewable units. In addition, power factor limitations on the CIG units can reduce their capability to provide reactive power. The increase in active power import aids in the improvement of the pre-contingency voltage levels which reduces the dynamic reactive power support necessary to maintain voltages during an event.

Case 3 (see Fig. 5-red), which includes both frequency and voltage transient constraints, indicates notable variations in both active and reactive power schedules. In this case, an hourly average of 0.975 MW active power and 2.089 MVar reactive power over the planning horizon is to be generated by the DERs in the MG to ensure a secure transient performance as compared to the Base case. Note that adherence to both frequency and voltage metrics is non-trivial especially given the competing requirements on the system power reserved by each of the transient metrics. That is, both the frequency and voltage-related metrics have sensitivity against both active and reactive power – thus, they might compete for resources. This is shown in Fig. 5 at hours 10, 11, 19 and 22 for active power and hours 10, 21 and 22 for reactive power when comparing Cases 1 and 2.

C. Transient Security Performance

The performance of the MG with respect to the transient security metrics (see Fig. 1) for frequency and voltage is presented in Figs. 6 and 7, respectively. The dashed red line indicates the limit below which a violation, and thus unit disconnection occurs during operation.

In the Base case, violations exist at various hours in both the frequency and voltage metrics indicating the potential disconnection of the DERs during an abrupt islanding event of the MG. Note that the Base case only takes into consideration the static security before and after MG islanding.

For Case 1 in Fig. 6, it is observed that the optimal solution obtained after power rescheduling at all hours indicates no violations of the transient frequency metrics. However, with
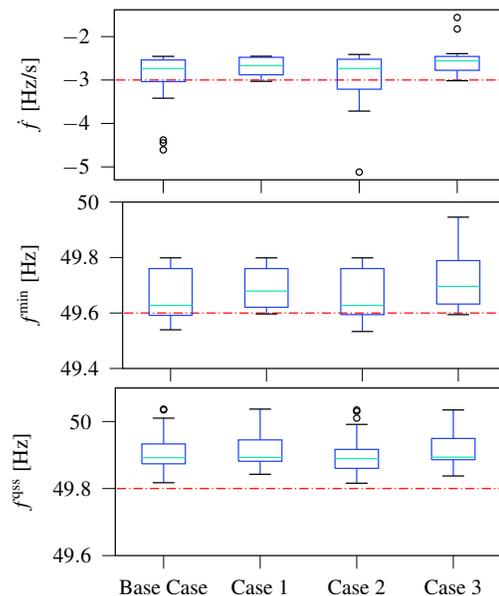
Fig. 6. Box-Plots showing the distribution of the transient frequency security metrics for all hours based on the CoI frequency model.
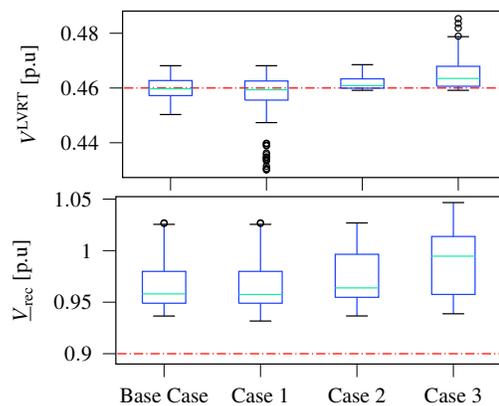
Fig. 7. Box-Plots showing the distribution of the transient voltage security metrics at the local generators for all hours.

regards to the voltage metrics in Case 1 indicated in Fig. 7 the LVRT limits remain violated for several hours in the planning horizon. A similar trend is observed in Case 2 wherein while the voltage metrics remain within the defined limits, the RoCoF limit is violated at different hours of the operational schedule. The separate analysis of either frequency or voltage
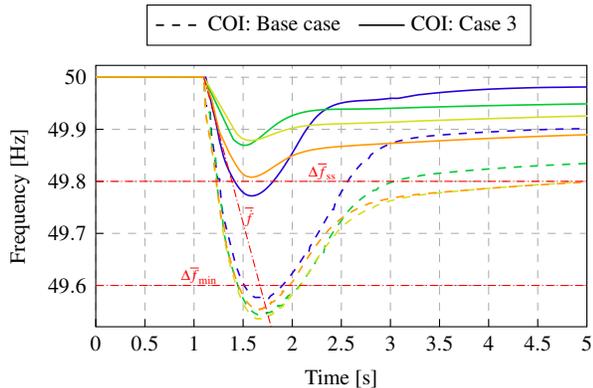
Fig. 8. CoI frequency trajectories during operation in hours 10 (blue), 19 (green), 20 (yellow), and 21 (orange) for the Base case and Case 3 operation with a disconnection at time 1 s.
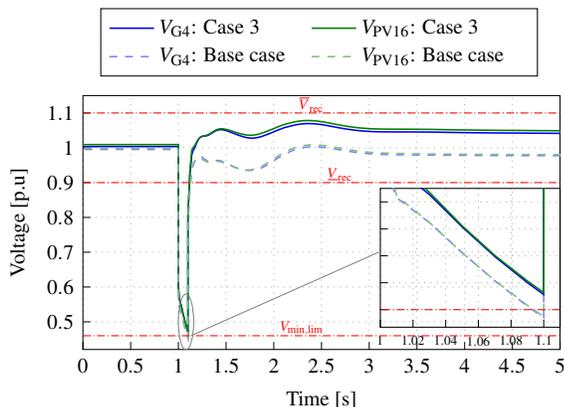
Fig. 9. Voltage trajectories at the terminals of SG G4 and CIG PV16 at hour 10 for unintentional islanding at time 1 s.

in the planning problem does not lead to a secure transition of the MG. Moreover, when only one type of the transient metrics is considered, Figs. 6 and Fig. 7 indicate further degradation in the system performance of the other metric type. Finally, the results for Case 3, indicate that both frequency and voltage transients are within the secure operation regions.

The power schedules computed for each hour are dynamically validated with the time-domain simulations (Step 2). Figures 8 and 9 show the frequency and voltage response respectively at hours 10, 19, 20, and 21 of the planning horizon with significant improvement in system performance for both metrics in Case 3. The associated active and reactive power response in the pre- and post-contingency states are indicated in Fig. 10. It is evident that the preventive rescheduling of power reserves greatly contributes to ensuring system degradation is minimised.

D. Effect to System Costs

The requirement for both static and dynamic security comes at a cost as indicated in Table II for the different case studies. In the Base case, the MG relies heavily on the cheaper power imported from the grid to ensure the satisfaction of the different steady-state operational constraints. The requirement for transient security during islanding demands increased power generation from the local resources available in the MG. In Cases 1 and 2, increments of 2867 $ and 2706 $ are observed, respectively, in comparison with the Base case. Note that
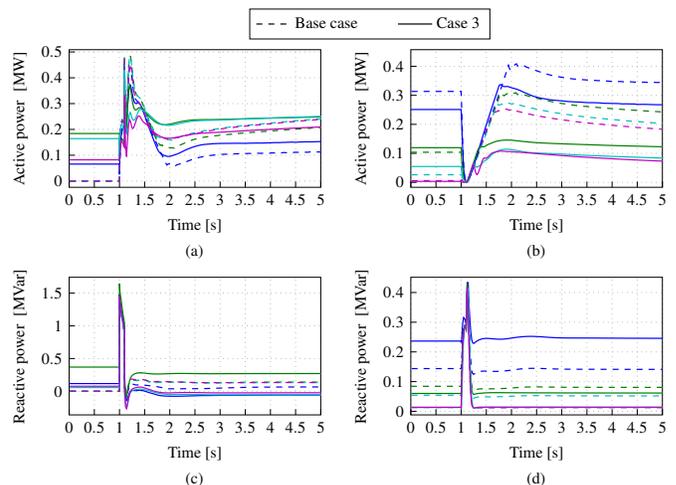
Fig. 10. Active power response at (a) SG G4 and (b) CIG PV16 and reactive power response at (c) SG G4 and (d) CIG PV16 in the Base case and Case 3 for hours 10 (blue), 19 (green), 20 (cyan) and 21 (pink).

TABLE II
OPERATIONAL COSTS INCURRED THE PLANNING CASE STUDIES

	Operation Cost [$]			
	Base	Case 1	Case 2	Case 3
Grid-connected	19203	22070	21909	38000
Islanded	0.0	0.0	0.0	0.0

in Case 1, higher-priced active power is more utilised as compared to Case 2 which heavily relies on reactive power. As CIG units are already maximised due to their negligible operational costs, the SG units provide the power reserves necessary thus increasing the total operational costs. The extra cost incurred due to preventive rescheduling reflects the system's security and resilience with respect to the islanding transients.

In Case 3, a significant extra cost of 18797 $ is observed. The active and reactive power scheduling requirements for the frequency and voltage metrics, shown to be competing in some hours and coherent in others (see Fig. 5), result in larger variations and higher costs. An overall increment of 15%, 14% and 98% is observed respectively for Cases 1, 2 and 3 as compared to the Base case to guarantee adherence to all transient security metrics.

V. CONCLUSION

A MG can ensure the power supply continuity during emergency grid conditions through its islanded operation capabilities. Its survivability is however dependent on its operational states remaining within secure regions in the pre-islanding, post-islanding, and transition periods. This paper proposes an algorithm to solve a transient-aware operational planning problem that ensures steady-state security and energy adequacy, as well as transient security during islanding. Linearized constraints related to the frequency and voltage security metrics are formulated (using time-domain simulations to derive sensitivity coefficients) and introduced as resilience cuts in the planning problem using an iterative approach. The performance of the proposed technique is demonstrated on a

medium-voltage distribution network with results indicating that neglecting the voltage and frequency transient security constraints or considering only one of them provides optimistic results with no security guarantees. Interactions between scheduling requirements for frequency and voltage metrics result in significant variations in active and reactive powers necessary to enhance system resilience and its associated costs. In the future, the algorithm will be extended to handle the uncertainty in load demand and renewable resource variations. Moreover, the use of embedded trajectory sensitivities during time-domain simulation can provide more accurate values for the influence of active and reactive power on the transient metrics.

References

[1] A. Hussain, V.-H. Bui, and H.-M. Kim, "Microgrids as a resilience resource and strategies used by microgrids for enhancing resilience," *Applied Energy*, vol. 240, pp. 56–72, 2019.

[2] M. Panteli and P. Mancarella, "The grid: Stronger, bigger, smarter?: Presenting a conceptual framework of power system resilience," *IEEE Power and Energy Magazine*, vol. 13, no. 3, pp. 58–66, 2015.

[3] A. H. Kasem Alaboudy, H. H. Zeineldin, and J. Kirtley, "Microgrid stability characterization subsequent to fault-triggered islanding incidents," *IEEE Trans. on Pow. Delivery*, vol. 27, no. 2, pp. 658–669, 2012.

[4] W. Zheng, P. Crossley, B. Xu, and H. Qi, "Transient stability of a distribution subsystem during fault-initiated switching to islanded operation," *Int. Journal of Elec. Pow. & Energy Sys.*, vol. 97, pp. 418–427, 2018.

[5] S. Eftekharnejad, V. Vittal, G. T. Heydt, B. Keel, and J. Loehr, "Impact of increased penetration of photovoltaic generation on power systems," *IEEE Trans. on Pow. Sys.*, vol. 28, no. 2, pp. 893–901, 2013.

[6] C. Gouveia, J. Moreira, C. L. Moreira, and J. A. Peças Lopes, "Coordinating storage and demand response for microgrid emergency operation," *IEEE Transactions on Smart Grid*, vol. 4, no. 4, pp. 1898–1908, 2013.

[7] A. Khodaei, "Microgrid optimal scheduling with multi-period islanding constraints," *IEEE Transactions on Power Systems*, vol. 29, no. 3, pp. 1383–1392, 2014.

[8] S. Karagiannopoulos, J. Gallmann, M. G. Vayá, P. Aristidou, and G. Hug, "Active distribution grids offering ancillary services in islanded and grid-connected mode," *IEEE Transactions on Smart Grid*, vol. 11, no. 1, pp. 623–633, 2020.

[9] I.-I. Avramidis, F. Capitanescu, S. Karagiannopoulos, and E. Vrettos, "A novel approximation of security-constrained optimal power flow with incorporation of generator frequency and voltage control response," *IEEE Transactions on Power Systems*, vol. 36, no. 3, pp. 2438–2447, 2021.

[10] Z. Chu and F. Teng, "Voltage stability constrained unit commitment in high ibg-penetrated power systems," 2021.

[11] H. Ahmadi and H. Ghasemi, "Security-constrained unit commitment with linearized system frequency limit constraints," *IEEE Transactions on Power Systems*, vol. 29, no. 4, pp. 1536–1545, 2014.

[12] F. Teng, V. Trovato, and G. Strbac, "Stochastic scheduling with inertia-dependent fast frequency response requirements," *IEEE Transactions on Power Systems*, vol. 31, no. 2, pp. 1557–1566, 2016.

[13] S. S. Guggilam, C. Zhao, E. Dall'Anese, Y. C. Chen, and S. V. Dhople, "Optimizing der participation in inertial and primary-frequency response," *IEEE Transactions on Power Systems*, vol. 33, no. 5, pp. 5194–5205, 2018.

[14] M. Paturet, U. Markovic, S. Delikaraoglou, E. Vrettos, P. Aristidou, and G. Hug, "Stochastic unit commitment in low-inertia grids," *IEEE Trans. on Pow. Sys.*, vol. 35, no. 5, pp. 3448–3458, 2020.

[15] Z. Chu, N. Zhang, and F. Teng, "Frequency-constrained resilient scheduling of microgrid: A distributionally robust approach," *IEEE Transactions on Smart Grid*, vol. 12, no. 6, pp. 4914–4925, 2021.

[16] Y. Zhang, C. Chen, G. Liu, T. Hong, and F. Qiu, "Approximating trajectory constraints with machine learning – microgrid islanding with frequency constraints," *IEEE Transactions on Power Systems*, vol. 36, no. 2, pp. 1239–1249, 2021.

[17] A. M. Nakiganda, S. Dehghan, and P. Aristidou, "Enhancing microgrid resilience and survivability under static and dynamic islanding constraints," in *2020 IEEE PES Innovative Smart Grid Technologies Europe (ISGT-Europe)*, 2020, pp. 539–543.

[18] A. M. Nakiganda, S. Dehghan, U. Markovic, G. Hug, and P. Aristidou, "A Stochastic-Robust Approach for Resilient Microgrid Investment Planning Under Static and Transient Islanding Security Constraints," *arXiv e-prints*, Jul. 2020.

[19] M. La Scala, M. Trovato, and C. Antonelli, "On-line dynamic preventive control: an algorithm for transient security dispatch," *IEEE Transactions on Power Systems*, vol. 13, no. 2, pp. 601–610, 1998.

[20] F. Capitanescu and T. Van Cutsem, "Preventive control of voltage security margins: a multicontingency sensitivity-based approach," *IEEE Transactions on Power Systems*, vol. 17, no. 2, pp. 358–364, 2002.

[21] M. Paramasivam, A. Salloum, V. Ajjarapu, V. Vittal, N. B. Bhatt, and S. Liu, "Dynamic optimization based reactive power planning to mitigate slow voltage recovery and short term voltage instability," *IEEE Trans. on Pow. Sys.*, vol. 28, no. 4, pp. 3865–3873, 2013.

[22] H. Liu, V. Krishnan, J. D. McCalley, and A. Chowdhury, "Optimal planning of static and dynamic reactive power resources," *IET Gen., Transn. Dist.*, vol. 8, no. 12, pp. 1916–1927, 2014.

[23] A. M. Nakiganda, T. Van Cutsem, and P. Aristidou, "Microgrid operational optimization with dynamic voltage security constraints," in *2021 IEEE Madrid PowerTech*, 2021, pp. 1–6.

[24] G. Hou and V. Vittal, "Trajectory sensitivity based preventive control of voltage instability considering load uncertainties," *IEEE Trans. on Pow. Sys.*, vol. 27, no. 4, pp. 2280–2288, 2012.

[25] European Commission, "Commission regulation (EU) 2016/631 of 14 April 2016 establishing a network code on requirements for grid connection of generators (Text with EEA relevance)," *Official Journal of the European Union*, vol. 112, pp. 1–68, Apr 2016.

[26] P. Kundur, *Power system stability and control*. New York: McGraw-Hill, 1994.

[27] M. Dreidy, H. Mokhlis, and S. Mekhilef, "Inertia response and frequency control techniques for renewable energy sources: A review," *Renewable and Sustainable Energy Reviews*, vol. 69, pp. 144–155, 2017. [Online]. Available: https://www.sciencedirect.com/science/article/pii/S1364032116309212

[28] U. Markovic, O. Stanojev, P. Aristidou, E. Vrettos, D. Callaway, and G. Hug, "Understanding small-signal stability of low-inertia systems," *IEEE Transactions on Power Systems*, vol. 36, no. 5, pp. 3997–4017, 2021.

[29] J. Morren, S. de Haan, W. Kling, and J. Ferreira, "Wind turbines emulating inertia and supporting primary frequency control," *IEEE Transactions on Power Systems*, vol. 21, no. 1, pp. 433–434, 2006.

[30] Turbine-governor models: Standard dynamic turbine-governor systems in neplan power system analysis tool. [Online]. Available: https://www.neplan.ch/wp-content/uploads/2015/08/Nep_TURBINES_GOV.pdf

[31] G. Chaspierre, P. Panciatici, and T. Van Cutsem, "Dynamic equivalent of a distribution grid hosting dispersed photovoltaic units," in *Proc. 10th Bulk Power Syst. Dyn. & Control Symp. (IREP)*, 2017, pp. 1–12.

[32] K. Kawabe, Y. Ota, A. Yokoyama, and K. Tanaka, "Novel dynamic voltage support capability of photovoltaic systems for improvement of short-term voltage stability in power systems," *IEEE Trans. on Power Sys.*, vol. 32, no. 3, pp. 1796–1804, 2017.

[33] IEEE, "Ieee recommended practice for excitation system models for power system stability studies," *IEEE Std 421.5-2016 (Revision of IEEE Std 421.5-2005)*, pp. 1–207, 2016.

[34] W. F. Feehery and P. I. Barton, "Dynamic optimization with state variable path constraints," *Computers & Chemical Engineering*, vol. 22, no. 9, pp. 1241–1256, 1998.

[35] L. T. Biegler and I. E. Grossmann, "Retrospective on optimization," *Computers & Chemical Engineering*, vol. 28, no. 8, pp. 1169–1192, 2004.

[36] S. Abhyankar, G. Geng, M. Anitescu, X. Wang, and V. Dinavahi, "Solution techniques for transient stability-constrained optimal power flow – part i," *IET Generation, Transmission & Distribution*, vol. 11, no. 12, pp. 3177–3185, 2017.

[37] G. Geng, S. Abhyankar, X. Wang, V. Dinavahi, and I. P. T. F. on Interfacing Techniques for Solution Tools, "Solution techniques for transient stability-constrained optimal power flow – part ii," *IET Generation, Transmission & Distribution*, vol. 11, no. 12, pp. 3186–3193, 2017.

[38] A. Ortega and F. Milano, "Impact of frequency estimation for vsc-based devices with primary frequency control," in *2017 IEEE PES Innovative Smart Grid Technologies Conference Europe (ISGT-Europe)*, 2017, pp. 1–6.

[39] F. Milano, F. Dörfler, G. Hug, D. J. Hill, and G. Verbič, "Foundations and challenges of low-inertia systems (invited paper)," in *2018 Power Systems Computation Conference (PSCC)*, 2018, pp. 1–25.

[40] F. Zhou and S. H. Low, "A note on branch flow models with line shunts," *IEEE Transactions on Power Systems*, vol. 36, no. 1, pp. 537–540, 2021.

[41] P. Kotsampopoulos, N. Hatziargyriou, B. Bletterie, and G. Lauss, "Review, analysis and recommendations on recent guidelines for the provision of ancillary services by distributed generation," in *2013 IEEE International Workshop on Inteligent Energy Systems (IWIES)*, 2013, pp. 185–190.

[42] J. Lopes, C. Moreira, and A. Madureira, "Defining control strategies for microgrids islanded operation," *IEEE Transactions on Power Systems*, vol. 21, no. 2, pp. 916–924, 2006.

[43] E. Kägi-Kolisnyc, "Distribution Management System Including Dispersed Generation and Storage in a Liberalized Market Environment," Ph.D. dissertation, EPFL, Lausanne, Switzerland, 2009.

[44] P. Aristidou, S. Lebeau, and T. Van Cutsem, "Power system dynamic simulations using a parallel two-level schur-complement decomposition," *IEEE Trans. on Power Sys.*, vol. 31, no. 5, pp. 3984–3995, 2016.

[45] W. E. Hart, J.-P. Watson, and D. L. Woodruff, "Pyomo: modeling and solving mathematical programs in python," *Mathematical Programming Computation*, vol. 3, no. 3, pp. 219–260, 2011.

[46] Gurobi Optimization, LLC, "Gurobi optimizer reference manual," 2020. [Online]. Available: http://www.gurobi.com

[47] Open power system data. [Online]. Available: https://doi.org/10.25832/time_series/2020-10-06

Agnes Marjorie Nakiganda (S'15-M'22) received the B.Sc. degree in Electrical Engineering from the Makerere University, Uganda, in 2011. She obtained the M.Sc. degree in Electrical Engineering and Renewable Energy Systems in 2015 and Ph.D. degree in Electronic And Electrical Engineering in 2022 from the University of Leeds, Leeds, UK. where she is currently working towards the Ph.D. degree since October 2018. She is currently a Postdoctoral researcher with the Center for Electric Power and Energy at the Technical University of Denmark (DTU). Her research interests include control and optimization of networks with a high penetration of converter-interfaced units and machine learning applications for power systems.

Petros Aristidou (S'10-M'15-SM'20) received a Diploma in Electrical and Computer Engineering from the National Technical University of Athens, Greece, in 2010, and a Ph.D. in Engineering Sciences from the University of Liège, Belgium, in 2015. He is currently a Lecturer in Sustainable Power Systems at the Cyprus University of Technology. His research interests include power system dynamics, control, and simulation.